Supporting Information

Podolec et al.

SI Materials and Methods

Hypocotyl length measurements. Quantification of hypocotyl length was performed as described previously (1). At least 60 seedlings for each genotype and experimental condition were aligned on plates, which were then scanned and hypocotyl length was measured using the NeuronJ plugin of ImageJ (2). Violin and box plots were generated using the ggplot2 package in R (3), and statistically different groups were determined using the Tukey HSD test from the agricolae package in R (4).

Extraction and analysis of anthocyanins and flavonoids. Anthocyanins were quantified from seedling extracts as described previously (5). Approximately 50 mg fresh weight of seedlings were ground and pigments were extracted in 250 µl methanol with 1% [v/v] HCl at 4°C for at least 1 h. Clear supernatants were collected, and absorbance was measured at 530 nm and 655 nm. The amount of anthocyanins was calculated as $(A_{530} - 0.25 * A_{655}) / m$, where m is the fresh weight of the seedlings.

Flavonol profiles were analyzed by high-performance thin layer chromatography (HPTLC) as previously described (6). In brief, 50 mg of seedlings were harvested, ground, and incubated with 100 µl of 80% [v/v] methanol on a shaker for 10 min at 70°C before centrifugation. Clear supernatants were then collected and 10 µl of samples was spotted on silica HPTLC plates using capillary tubes. The methanolic extracts were then separated in a mobile phase consisting of a mixture of 5 ml ethyl acetate, 600 µl formic acid, 600 µl acetic acid glacial, and 1.3 ml water. After migration, the plate was dried and the flavonol staining was revealed under a 365-nm UV lamp after spraying the chromatogram with a 1% [w/v] diphenylboric acid 2-aminoethylester (DPBA; Roth) solution in 80% [v/v] methanol.

Immunoblot analysis. For analysis of protein levels by immunoblotting, proteins were extracted from seedlings using an extraction buffer consisting of 50 mM Na-phosphate pH 7.4, 150 mM NaCl, 10% [v/v] glycerol, 5 mM EDTA, 0.1% [v/v] Triton X-100, 1 mM DTT, 2 mM Na_3VO_4, 2 mM NaF, 1% [v/v] Protease Inhibitor Cocktail (Sigma), and 50 µM MG132 (7).

To determine the dimer/monomer status of UVR8 by SDS-PAGE, proteins were extracted in an extraction buffer composed of 150 mM NaCl, 50 mM Tris-HCl pH 7.6, 2 mM EDTA, 1% [v/v] Igepal (Sigma), 1% [v/v] Protease Inhibitor Cocktail (Sigma), 10 μM MG132, and 10 μM ALLN (VWR) (8). Extracts were then loaded on SDS-PAGE gels without prior heat denaturation and gels were exposed to broadband UV-B for 30 min before transfer, as described previously (9).

For HY5 immunoblots, the following extraction buffer was used: 50 μM EDTA, 0.1 M Tris-HCl pH 8, 0.7% [w/v] SDS, 10 mM NaF, cOmplete^{TM} EDTA-free Protease Inhibitor Cocktail Tablet (Roche), 1 mM DTT, 0.25 M NaCl, 15 mM β-glycerolphosphate, and 15 mM p-nitrophenyl phosphate (10).

Following electrophoretic separation in SDS-PAGE gels, proteins were transferred to PVDF membranes (Roth) according to the manufacturer's instructions (iBlot dry blotting system, Thermo Fisher Scientific); however, to analyze RUP2 levels, proteins were liquid-transferred to nitrocellulose membranes (Bio-Rad). Membranes were blocked in 10% [w/v] milk, except for HY5 immunoblots, which were blocked by drying the membrane.

anti-UVR8$^{(426–440)}$ (11), anti-UVR8$^{(410-424)}$ (8), anti-UVR8$^{(1–15)}$ (12), anti-GFP (Living Colors® A.v. Monoclonal Antibody, JL-8; Clontech), anti-CHS (sc-12620; Santa Cruz Biotechnology), anti-UGPase (AS05086, Agrisera), anti-Histone H3 (ab1791, Abcam), anti-actin (A0480; Sigma-Aldrich), anti-HY5 (10), anti-COP1 (8) and anti-RUP2 (7) were used as primary antibodies, and corresponding horseradish peroxidase-conjugated anti-rabbit, anti-mouse, and anti-goat (Dako) immunoglobulins were used as secondary antibodies. Signal detection was done on an Amersham Imager 680 camera system (GE Healthcare) using the ECL Select Western Blotting Detection Reagent (GE Healthcare).

Co-immunoprecipitation. Protein complexes were extracted using a buffer composed of 50 mM Tris pH 7.6, 75 mM NaCl, 10% [v/v] glycerol, 5 mM EDTA, 15 mM EGTA, 0.1% [v/v] Igepal, 10 mM benzamidine, 10 μM leupeptin, 2 mM Na_3VO_4, 25 mM NaF, 1 mM PMSF, 50 mM β-glycerophosphate, 1% [v/v] Protease Inhibitor Cocktail (Sigma) and 50 μM MG132. YFP-tagged proteins were immunoprecipitated using the μMACS GFP Isolation Kit (Miltenyi Biotech), with washes performed using the extraction buffer.

Cell fractionation and purification of nuclear proteins. Separation of nuclear and cytosolic fractions was performed as previously described (13). In short, plant material was ground and used for extraction in a buffer composed of 20 mM Tris pH 7.6, 25% [v/v] glycerol, 20 mM

KCl, 2 mM EDTA, 2.5 mM $MgCl_2$, 250 mM sucrose, 1 mM DTT and 1 mM PMSF. The extract was filtered through three layers of micracloth and centrifuged for 10 min at 1500 g at 4°C. The supernatant was separated as the cytosolic fraction whereas the pellet containing nuclei was washed at least three times in the resuspension buffer composed of 50 mM Tris pH 7.6, 25% [v/v] glycerol, 2.5 mM $MgCl_2$ and 0.2% [v/v] Triton X-100. Finally, the nuclear pellet was washed in resuspension buffer without Trition X-100 and nuclear proteins were extracted by heat-denaturation in SDS-PAGE loading buffer.

Protein crosslinking. Crosslinking experiments were performed as described before (9). Proteins were extracted from seedlings in PBS containing 0.1% [v/v] Igepal, 1 mM PMSF, 10 mM leupeptine, 1% [v/v] protease inhibitor cocktail for plants (Sigma), 10 μM MG132, and 10 μM ALLN (VWR). Extracts were then centrifuged and clear supernatants were incubated with 2 mM dithiobis(succinimidyl propionate) (DSP; ThermoFisher) for 30 min at 4°C on a rotary shaker. Crosslinking was then quenched with 50 mM Tris pH 7.6 for 15 min at room temperature. Samples were then heat denatured in SDS-PAGE loading buffer without reducing agent. To reverse crosslinking, 5% [v/v] β-mercaptoethanol was added prior to heat-based denaturation.

Yeast two-hybrid (Y2H) analysis. To test the UVR8–COP1 interaction, *COP1* was inserted into pGADT7-GW (14, 15) and *UVR8*, $UVR8^{G101S}$, $UVR8^{W285A}$, $UVR8^{G101S,W285A}$, $UVR8^{W285F}$, $UVR8^{G101S,W285F}$, and $UVR8^{D96N,D107N}$ were cloned into pBTM116-D9-GW (15, 16). The L40 yeast stain (17) was used for transformation using the lithium acetate–based transformation protocol (18).

To test the interaction of UVR8 with RUP2, *RUP2* was cloned into pGBKT7-GW (19) and transformed into the Y2H Gold strain (Clontech). *UVR8* and $UVR8^{G101S}$ were introduced into pGADT7-GW (14) and transformed into the Y187 strain (20). The relevant pairs were then combined by mating.

Transformed yeast cells were selected on SD/-Trp/-Leu medium (Foremedium) for non-selective growth and on a SD/-Trp/-Leu/-His medium for selective growth. To quantify the interactions using the LacZ reporter, yeast strains were grown for 2 d on non-selective medium and the β-galactosidase enzymatic activity was determined in an assay using red-β-D-galactopyranoside (CPRG, Roche Applied Science) as substrate (Yeast Protocols Handbook, Clontech). For UV-B treatments, yeast cells were irradiated with 1.5 μmol m^{-2} s^{-1} of narrow-band UV-B provided by Philips TL20W/01RS tubes.

Protein purification from Sf9 cell cultures. *Spodoptera frugiperda* Sf9 cells (Thermofisher) were cultured in Sf-4 Baculo Express insect cell medium (Bioconcept, Switzerland).

Each of the recombinant $COP1^{349–675}$, UVR8 full-length, and $UVR8^{12–381}$ proteins were produced as described before (1). The desired Arabidopsis full-length or truncated coding sequence was PCR amplified or NcoI/NotI digested from codon-optimized genes (Geneart) for expression in Sf9 cells. Mutant UVR8 constructs were produced using an enhanced plasmid mutagenesis protocol (21). All were cloned into a modified pFastBac (Geneva Biotech) insect cell expression vector via NcoI/NotI restriction enzyme sites or by Gibson assembly (22). The modified pFastBac vector contains a tandem N-terminal His_{10}-Twin-Strep-tags followed by a TEV (tobacco etch virus protease) cleavage site.

pFastBac constructs were transformed into DH10MultiBac cells (Geneva Biotech), following which white colonies indicating successful recombination were selected and bacmids were purified by the alkaline lysis method. Sf9 cells were transfected with the desired bacmid with Profectin (AB Vector). eYFP-positive cells were observed after 1 week and subjected to one round of viral amplification. Amplified, untitred P2 virus (between 5–10% culture volume) was used to infect Sf9 cells at a density between 1–2 x 10^6 cells/ml. Cells were incubated for 72 h at 28°C before the cell pellet was harvested by centrifugation at 2000 × *g* for 20 min and stored at –20°C.

Pellets from every liter of Sf9 cell culture were dissolved in 25 ml of buffer A (300 mM NaCl, 20 mM HEPES 7.4, 2 mM β-ME), supplemented with 10% [v/v] glycerol, 5 µl Turbonuclease, and 1 Roche cOmplete™ protease inhibitor tablet. Dissolved pellets were lysed by sonication and insoluble materials were separated by centrifugation at 60,000 × *g* for 1 h at 4°C. The supernatant was filtered through tandem 1-µm and 0.45-µm filters before Ni^{2+}-affinity purification (HisTrap excel, GE Healthcare). Ni^{2+}-bound proteins were washed with buffer A and eluted directly onto a coupled Strep-Tactin Superflow XT column (IBA) by buffer B (500 mM NaCl, 500 mM imidazole pH 7.4, 20 mM HEPES pH 7.4). Tandem-Strep-tagged-bound proteins on the Strep-Tactin column were washed with buffer A and eluted with 1x Buffer BXT (IBA). Proteins were cleaved overnight at 4°C with TEV protease. Cleaved proteins were subsequently purified from the protease and affinity tag by a second Ni^{2+}-affinity column or by gel filtration on a Superdex 200 Increase 10/300 GL column (GE Healthcare). Proteins were concentrated to 3–10 mg/ml and either used immediately or aliquoted and quickly frozen at –80°C. Typical purifications were from pellets of 2–5 liters of insect cell culture. All protein concentrations were measured by absorption at 280 nm and

calculated from their molar extinction coefficients. Molecular weights of all proteins were confirmed by MALDI-TOF mass spectrometry. SDS-PAGE gels to assess protein purity are shown in *SI Appendix*, Fig. S14. For UVR8 monomerization and activation by UV-B, purified UVR8 proteins were exposed for 60 min at max intensity (69 mA) under UV-B LEDs (Roithner Lasertechnik GmbH) on ice.

Analytical size-exclusion chromatography. Gel filtration experiments were performed using a Superdex 200 Increase 10/300 GL column (GE Healthcare) pre-equilibrated in 150 mM NaCl, 20 mM HEPES 7.4, and 2 mM β-ME. 500 µl of the respective protein solution (~4 µM per protein) was loaded sequentially onto the column and elution at 0.75 ml/min was monitored by UV absorbance at 280 nm.

***In vitro* methylation.** 150 µl of 4 mg/ml COP1/UVR8$^{12–381,\ D96N,D107N}$ complex was diluted to 500 µl using buffer (150 mM NaCl, 20 mM HEPES pH 7.4). 20 µl of 1 M dimethylaminoborane (DMAB) and 40 µl of formaldehyde was added to the protein mixture at 4°C and left rotating for 2 h. The addition of DMAB and formaldehyde was repeated once. 10 µl of 1 M DMAB was subsequently added and the mixture was left on ice overnight. The reaction was quenched with 125 µl of 1 M Tris pH 8, concentrated to 500 µl and loaded onto a Superdex 200 Increase 10/300 GL column. Methylation was confirmed by MALDI-TOF mass spectrometry with ~13 free amines methylated on UVR8^{D96N,D107N}.

Protein crystallization and data collection. Crystals of truncated UVR8 (residues 12–381) mutants were grown in sitting drops and appeared after several days (UVR8^{D96N,D107N}, UVR8^{D96N,D107N,W285A}) to 1 year (UVR8^{G101S,W285A}) at 20°C in drops where 5 mg/ml of UVR8^{D96N,D107N,W285A} or UVR8^{G101S,W285A} was mixed in a protein:buffer ratio of 1:1. UVR8^{D96N,D107N,W285A} crystals formed in 0.2 M $NaNO_3$, 22% [w/v] PEG 3,350, whereas UVR8 UVR8^{G101S,W285A} crystals formed in 0.1 M Bis-Tris propane pH 8.5, 0.2 M $NaNO_3$, 20% [w/v] PEG 3,350. UVR8^{D96N,D107N} crystals formed when *in vitro* methylated COP1/UVR8^{D96N,D107N} complex at 1.8 mg/ml was mixed in a ratio of 2:1 protein:buffer in 0.1 M Tris pH 8.5, 0.1 M NaCl, 30% [w/v] PEG 4,000. Crystals were harvested and cryoprotected in mother liquor supplemented with 25% [v/v] glycerol for UVR8^{D96N,D107N} and UVR8^{G101S,W285A} or with 20% [w/v] PEG 400 for UVR8^{D96N,D107N,W285A} and frozen in liquid nitrogen.

Native datasets were collected at beam line PX-III of the Swiss Light Source (Villigen) with λ=1.03 Å. All datasets were processed with XDS (23) and scaled with AIMLESS as implemented in the CCP4 suite (24).

Crystallographic structure solution and refinement. The structures of the mutant UVR8 versions were solved by molecular replacement as implemented in the program Phaser (25), using PDB-ID 4D9S as the initial search model. The final structures were determined after iterative rounds of model-building in COOT (26), followed by refinement in REFMAC5 (27) and phenix.refine (28). Final statistics were generated using phenix.table_one. Structural diagrams were rendered in UCSF Chimera (29) and UCSF ChimeraX (30).

Grating-coupled interferometry (GCI). The Creoptix WAVE system (Creoptix AG), a label-free surface biosensor, was used to perform GCI experiments. All experiments were performed on 2PCH or 4PCH WAVEchips (quasi-planar polycarboxylate surface; Creoptix AG). After a borate buffer conditioning (100 mM sodium borate pH 9.0, 1 M NaCl; Xantec) COP1 (ligand) was immobilized on the chip surface using standard amine-coupling: 7-min activation (1:1 mix of 400 mM *N*-(3-dimethylaminopropyl)-*N′*-ethylcarbodiimide hydrochloride and 100 mM *N*-hydroxysuccinimide (both Xantec)), injection of COP1 (10 µg/ml) in 10 mM sodium acetate pH 5.0 (Sigma) until the desired density was reached, and final quenching with 1 M ethanolamine pH 8.0 for 7 min (Xantec). For a typical experiment, the analyte (UVR8) was injected in a 1:3 dilution series in 150 mM NaCl, 20 mM HEPES 7.4, 2 mM β-ME at 25°C. Blank injections were used for double referencing and a dimethylsulfoxide (DMSO) calibration curve for bulk correction. Analysis and correction of the obtained data was performed using the Creoptix WAVEcontrol software (applied corrections: X and Y offset; DMSO calibration; double referencing) and a one-to-one binding model or a heterogenous ligand model with bulk correction was used to fit all experiments. Data of GCI binding assays are reported with errors as indicated in their figure legends.

References

1. K. Lau, R. Podolec, R. Chappuis, R. Ulm, M. Hothorn, Plant photoreceptors and their signaling components compete for COP1 binding via VP peptide motifs. *EMBO J.* **38**, e102140 (2019).
2. E. Meijering, et al., Design and validation of a tool for neurite tracing and analysis in fluorescence microscopy images. *Cytometry Part A* **58A**, 167-176 (2004).
3. H. Wickham (2009) *ggplot2: Elegant Graphics for Data Analysis* (Springer-Verlag New York).
4. F. de Mendiburu (2019) agricolae: Statistical Procedures for Agricultural Research.

5. R. Yin, et al., Feedback inhibition of the general phenylpropanoid and flavonol biosynthetic pathways upon a compromised flavonol-3-O-glycosylation. *J. Exp. Bot.* **63**, 2465-2478 (2012).
6. R. Stracke, et al., The Arabidopsis bZIP transcription factor HY5 regulates expression of the *PFG1/MYB12* gene in response to light and ultraviolet-B radiation. *Plant Cell Environ.* **33**, 88-103 (2010).
7. A. B. Arongaus, et al., Arabidopsis RUP2 represses UVR8-mediated flowering in noninductive photoperiods. *Genes Dev.* **32**, 1332-1343 (2018).
8. M. Heijde, R. Ulm, Reversion of the Arabidopsis UV-B photoreceptor UVR8 to the homodimeric ground state. *Proc. Natl. Acad. Sci. USA* **110**, 1113-1118 (2013).
9. L. Rizzini, et al., Perception of UV-B by the Arabidopsis UVR8 protein. *Science* **332**, 103-106 (2011).
10. A. Oravecz, et al., CONSTITUTIVELY PHOTOMORPHOGENIC1 is required for the UV-B response in Arabidopsis. *Plant Cell* **18**, 1975-1990 (2006).
11. J. J. Favory, et al., Interaction of COP1 and UVR8 regulates UV-B-induced photomorphogenesis and stress acclimation in Arabidopsis. *EMBO J.* **28**, 591-601 (2009).
12. R. Yin, A. B. Arongaus, M. Binkert, R. Ulm, Two distinct domains of the UVR8 photoreceptor interact with COP1 to initiate UV-B signaling in Arabidopsis. *Plant Cell* **27**, 202-213 (2015).
13. R. Yin, M. Y. Skvortsova, S. Loubery, R. Ulm, COP1 is required for UV-B-induced nuclear accumulation of the UVR8 photoreceptor. *Proc. Natl. Acad. Sci. USA* **113**, E4415-E4422 (2016).
14. K. Marrocco, et al., Functional analysis of EID1, an F-box protein involved in phytochrome A-dependent light signal transduction. *Plant J.* **45**, 423-438 (2006).
15. M. Heijde, et al., Constitutively active UVR8 photoreceptor variant in Arabidopsis. *Proc. Natl. Acad. Sci. USA* **110**, 20326-20331 (2013).
16. U. Stelzl, et al., A human protein-protein interaction network: a resource for annotating the proteome. *Cell* **122**, 957-968 (2005).
17. A. B. Vojtek, S. M. Hollenberg (1995) Ras-Raf interaction: two-hybrid analysis. *Methods in Enzymology*, (Academic Press), Vol 255, pp 331-342.
18. R. D. Gietz (2014) Yeast transformation by the LiAc/SS carrier DNA/PEG method. *Yeast Genetics: Methods and Protocols*, eds Smith JS & Burke DJ (Springer New York, New York, NY), pp 1-12.
19. Q. Lu, et al., Arabidopsis homolog of the yeast TREX-2 mRNA export complex: components and anchoring nucleoporin. *Plant J.* **61**, 259-270 (2010).
20. J. Wade Harper, G. R. Adami, N. Wei, K. Keyomarsi, S. J. Elledge, The p21 Cdk-interacting protein Cip1 is a potent inhibitor of G1 cyclin-dependent kinases. *Cell* **75**, 805-816 (1993).
21. H. Liu, J. H. Naismith, An efficient one-step site-directed deletion, insertion, single and multiple-site plasmid mutagenesis protocol. *BMC Biotechnol.* **8**, 91 (2008).
22. D. G. Gibson, et al., Enzymatic assembly of DNA molecules up to several hundred kilobases. *Nat. Methods* **6**, 343-345 (2009).
23. W. Kabsch, Automatic processing of rotation diffraction data from crystals of initially unknown symmetry and cell constants. *J. Appl. Cryst.* **26**, 795-800 (1993).
24. M. D. Winn, et al., Overview of the CCP4 suite and current developments. *Acta Crystallogr. D Biol. Crystallogr.* **67**, 235-242 (2011).
25. A. J. McCoy, et al., Phaser crystallographic software. *J. Appl. Cryst.* **40**, 658-674 (2007).
26. P. Emsley, K. Cowtan, Coot: model-building tools for molecular graphics. *Acta Crystallogr. D Biol. Crystallogr.* **60**, 2126-2132 (2004).
27. G. N. Murshudov, et al., REFMAC5 for the refinement of macromolecular crystal structures. *Acta Crystallogr. D Biol. Crystallogr.* **67**, 355-367 (2011).
28. P. D. Adams, et al., PHENIX: a comprehensive Python-based system for macromolecular structure solution. *Acta Crystallogr. D Biol. Crystallogr.* **66**, 213-221 (2010).
29. E. F. Pettersen, et al., UCSF Chimera—A visualization system for exploratory research and analysis. *J. Comput. Chem.* **25**, 1605-1612 (2004).

30. T. D. Goddard, et al., UCSF ChimeraX: Meeting modern challenges in visualization and analysis. *Protein Sci.* **27**, 14-25 (2018).
31. C. Cloix, et al., C-terminal region of the UV-B photoreceptor UVR8 initiates signaling through interaction with the COP1 protein. *Proc. Natl. Acad. Sci. USA* **109**, 16366-16370 (2012).
32. H. Gruber, et al., Negative feedback regulation of UV-B-induced photomorphogenesis and stress acclimation in Arabidopsis. *Proc. Natl. Acad. Sci. USA* **107**, 20132-20137 (2010).
33. A. B. Arongaus, et al., Arabidopsis RUP2 represses UVR8-mediated flowering in noninductive photoperiods. *Genes Dev.* **32**, 1332-1343 (2018).

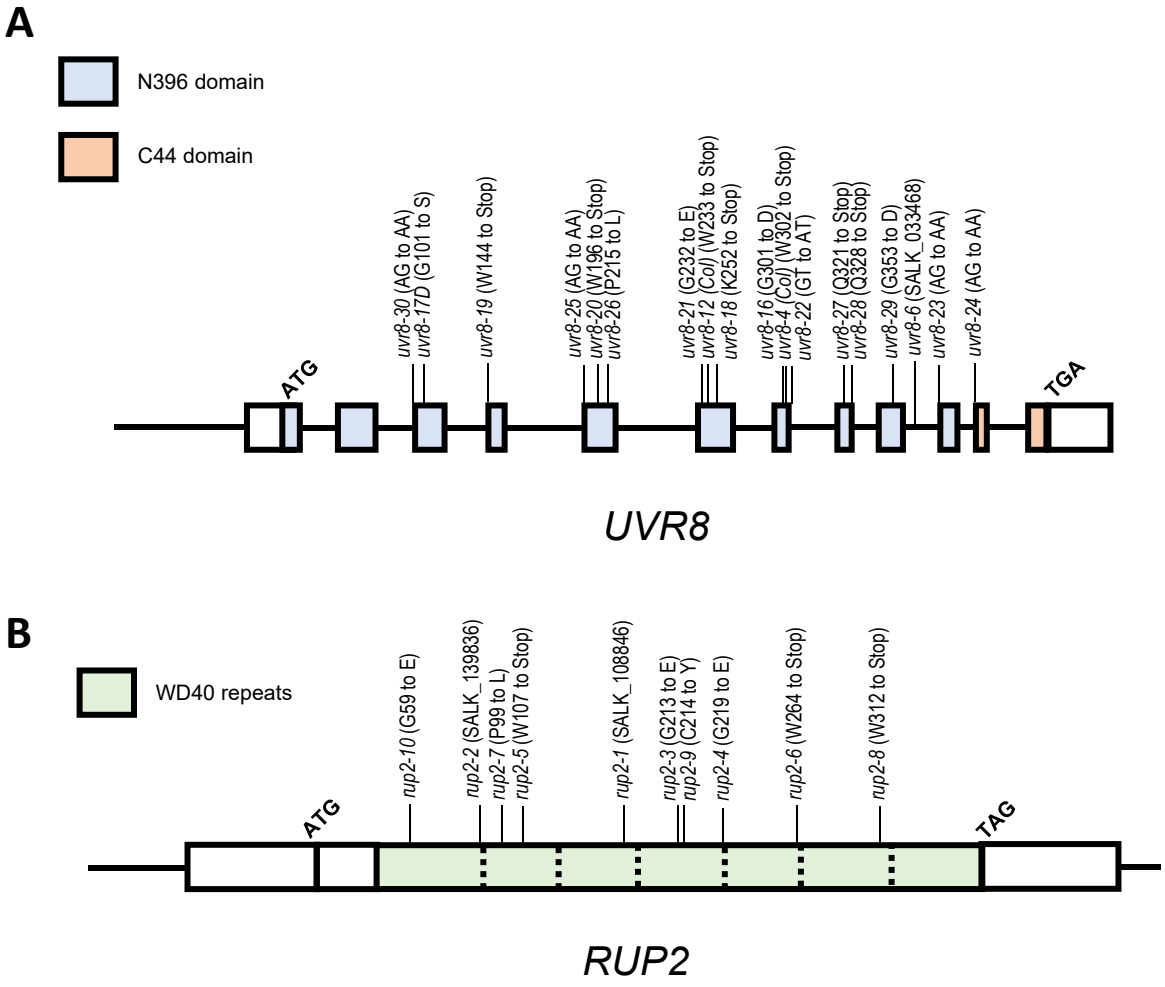

Fig. S1. Novel *uvr8* and *rup2* loss-of-function alleles. **(A)** Structure of the *UVR8* gene and new mutant alleles. Boxes indicate exons. The sequence corresponding to the N396 domain is colored in blue, the C44 domain is in orange (16). Novel alleles identified in the hypocotyl length–based screen are indicated (Col accession), in addition to the previously characterized *uvr8-6* T-DNA insertion mutant (11), and already known alleles previously described in other accessions: *uvr8-4* (originally reported in L*er*) (31) and *uvr8-12* (originally reported in Ws) (11). Additionally *uvr8-17D* is indicated. **(B)** Structure of the *RUP2* gene and new mutant alleles. Boxes indicate exons. The sequence colored in green represents the seven WD40 repeats (separated by dashed lines). The T-DNA insertion lines *rup2-1* (32) and *rup2-2* (33) are indicated, as well as all novel alleles.

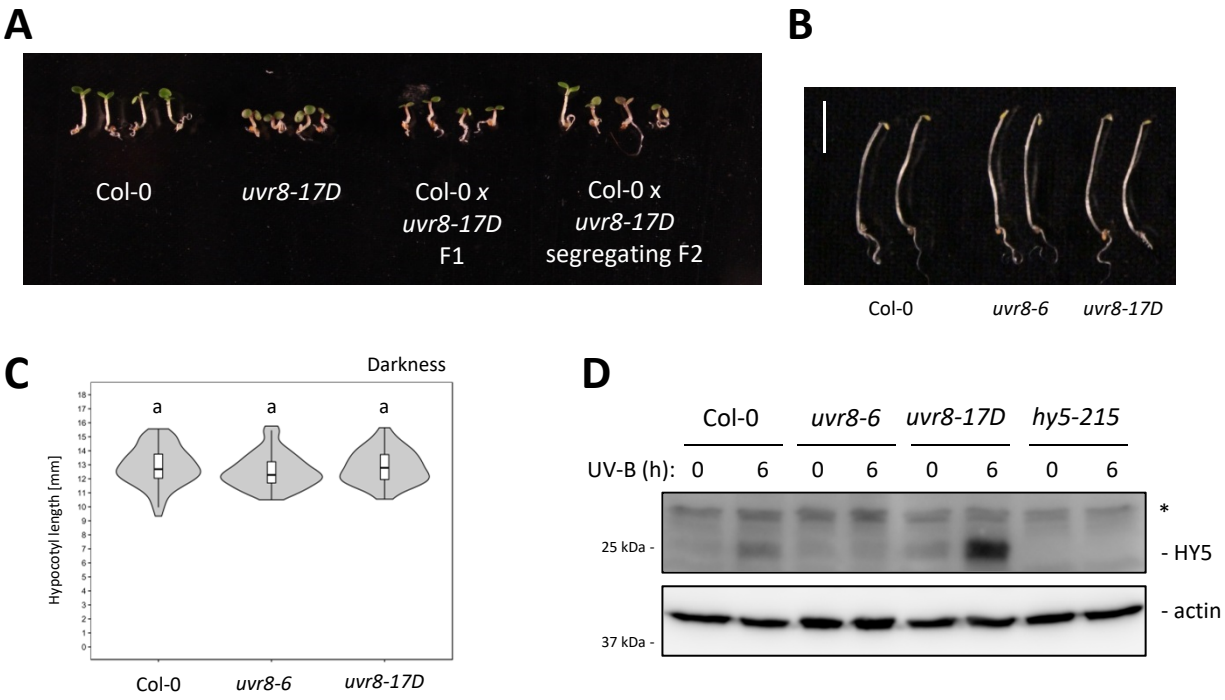

Fig. S2. Characterization of the *uvr8-17D* allele. **(A)** Representative images of the seedling phenotypes of wild type (Col-0), *uvr8-17D*, and F1 as well as segregating F2 progeny of a Col-0 x *uvr8-17D* cross, following seedling growth in white light supplemented with UV-B. **(B)** Representative images of wild-type, *uvr8-6*, and *uvr8-17D* seedlings grown in darkness. Bar = 5 mm. **(C)** Quantification of hypocotyl length of 4-d-old seedlings grown in darkness, representing genotypes described in (B) (*N* > 60). Shared letters indicate no statistically significant difference in the means (*P* > 0.05). **(D)** Immunoblot analysis of HY5 and actin (loading control) protein levels in wild-type, *uvr8-6*, *uvr8-17D*, and *hy5-215* seedlings grown in white light for 4 d, and either exposed or not exposed to supplemental UV-B for 6 h. Asterisk indicates nonspecific cross-reacting bands.

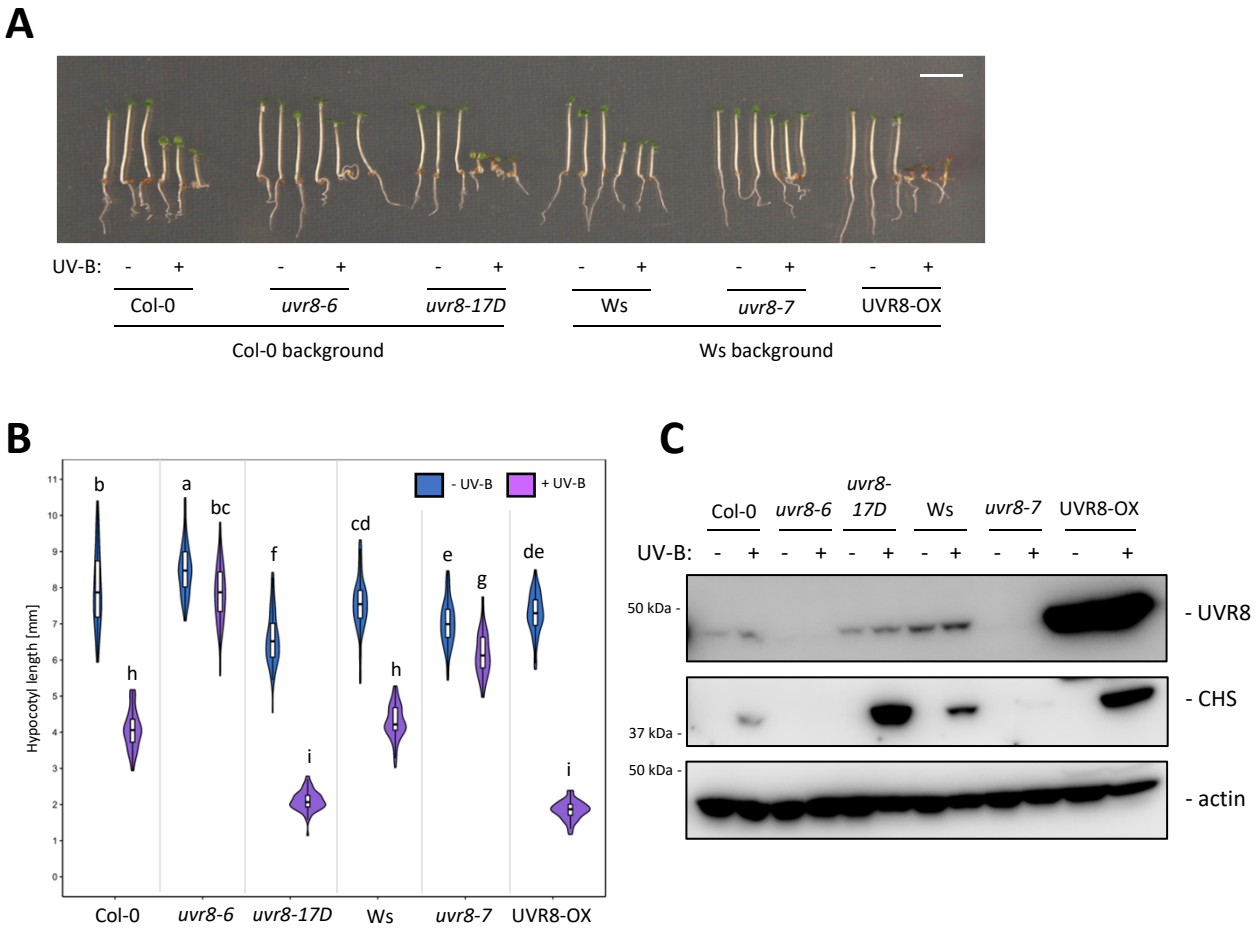

Fig. S3. Comparison of *uvr8-17D* and UVR8-OX. **(A)** Representative images of wild-type (Col-0), *uvr8-6*, *uvr8-17D*, wild-type (Ws), *uvr8-7*, and *uvr8-7*/Pro$_{35S}$:UVR8 (UVR8-OX) seedlings grown for 4 d in white light or white light supplemented with UV-B. Bar = 5 mm. **(B)** Quantification of hypocotyl length of seedlings described in (A) (N > 60). Shared letters indicate no statistically significant difference in the means (P > 0.05). **(C)** Immunoblot analysis of UVR8, CHS, and actin (loading control) protein levels in seedlings grown as described in (A).

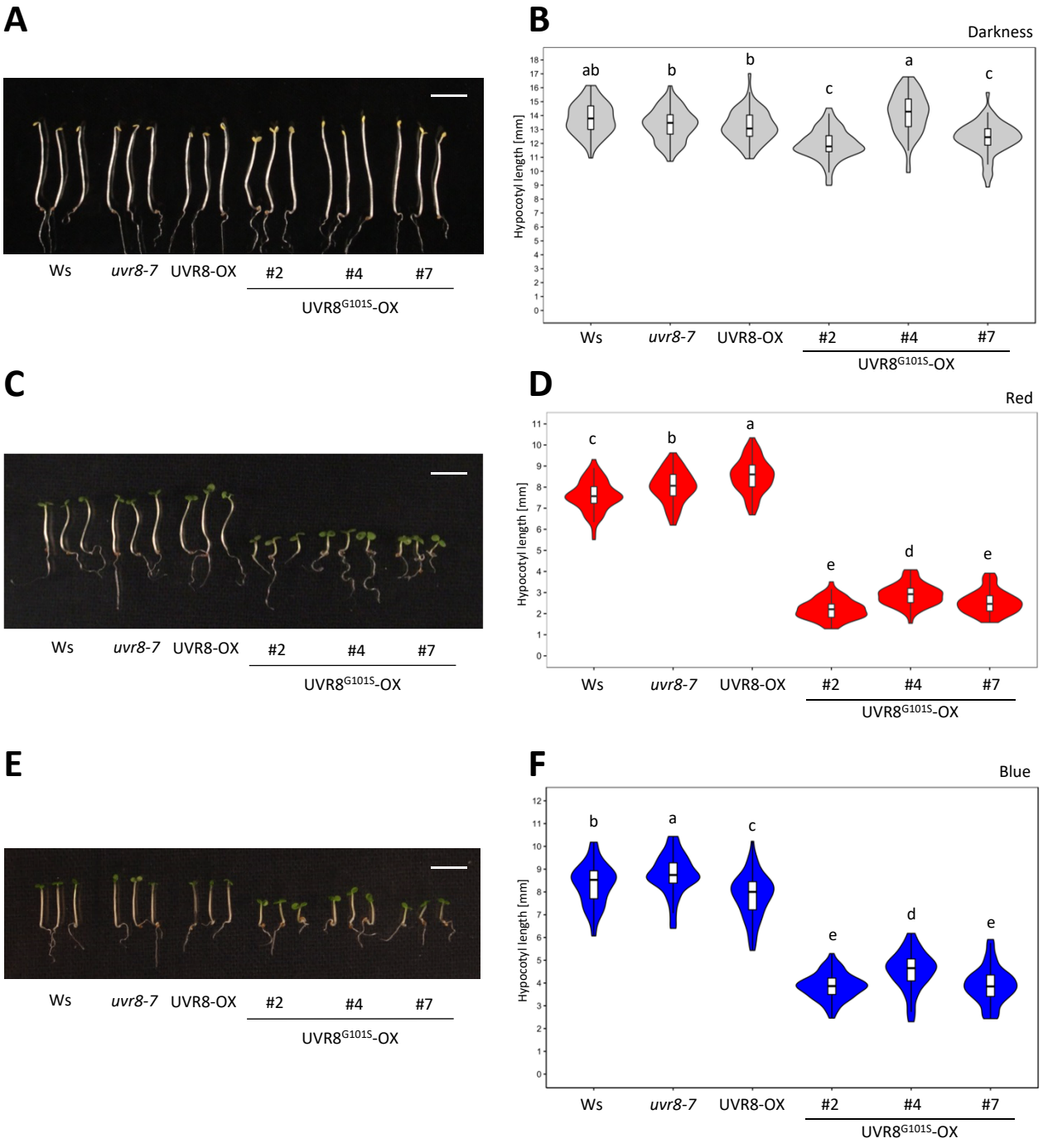

Fig. S4. UVR8^{G101S} overexpression lines show weak constitutive photomorphogenesis. **(A,C,E)** Representative images of seedlings of wild type (Ws), *uvr8-7*, *uvr8-7*/Pro$_{35S}$:UVR8 (UVR8-OX), and three independent *uvr8-7*/Pro$_{35S}$:UVR8^{G101S} (UVR8^{G101S}-OX #2, #4, and #7) lines grown **(A)** in darkness, **(C)** under 30 µmol m^{-2} s^{-1} of red light, or **(E)** under 5 µmol m^{-2} s^{-1} of blue light. Bar = 5 mm. **(B,D,F)** Quantification of hypocotyl length of seedlings described in (A,C,E) respectively (N > 60). Shared letters indicate no statistically significant difference in the means (P > 0.05).

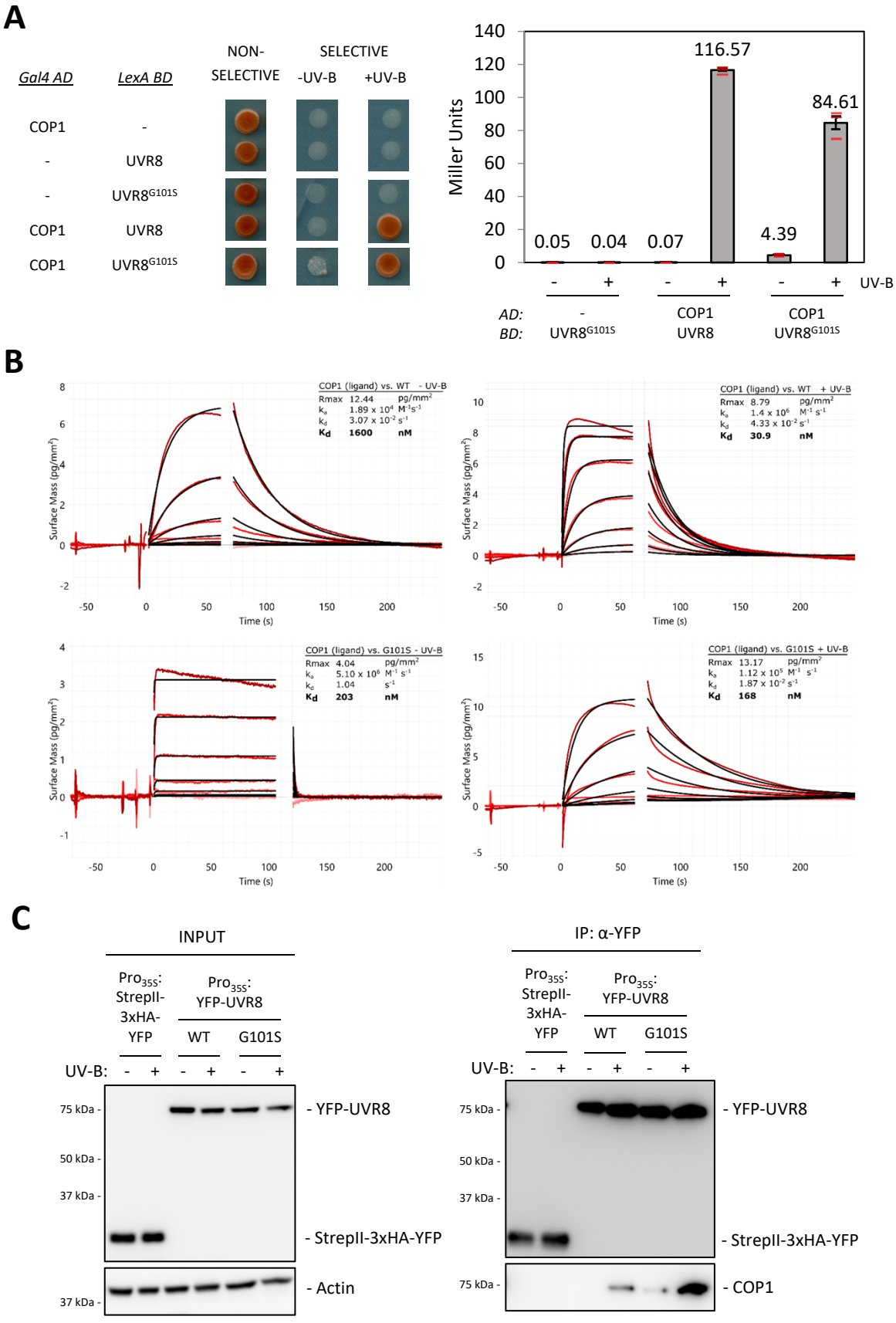

Fig. S5. UVR8^{G101S} interacts with COP1 in a UV-B-dependent manner. **(A)** Y2H analyses of the interactions between COP1 and UVR8/UVR8^{G101S} in the presence or absence of UV-B. Left: growth assay on selective SD/-Trp/-Leu/-His medium. Right: quantitative β-galactosidase assay. AD, activation domain; BD, DNA binding domain. **(B)** Binding kinetics of full-length UVR8 and UVR8^{G101S} versus the COP1 WD40 domain obtained by GCI experiments. Sensorgrams of protein injected are shown in red, with their respective heterogenous ligand binding model fits in black. The following amounts were typically used: ligand: COP1 (2,000 pg/mm^2); analyte: UVR8 (2 µM highest concentration). ka = association rate constant, kd = dissociation rate constant, Kd = dissociation constant. **(C)** Coimmunoprecipitation of COP1 using anti-GFP coupled beads in extracts from Col-0/Pro$_{35S}$:StrepII-3xHA-YFP (negative control), Col-0/Pro$_{35S}$:YFP-UVR8, and Col-0/Pro$_{35S}$:YFP-UVR8^{G101S} lines. Five-day-old seedlings were treated or not with 24h supplemental UV-B followed by a saturating 15 min UV-B pulse. IP = immunoprecipitation.

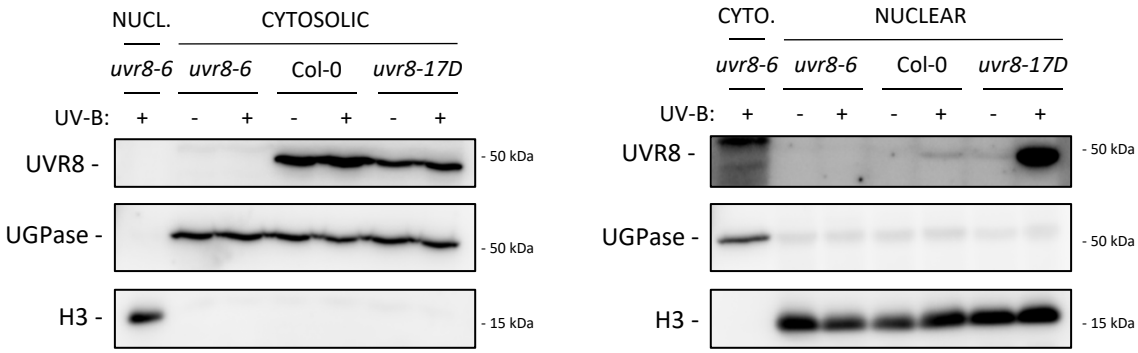

Fig. S6. Immunoblot analysis of UVR8, UGPase (cytosolic marker) and H3 (nuclear marker) levels in cytosolic and nuclear extracts from 4-day-old wild type (Col-0), *uvr8-6* and *uvr8-17D* seedlings grown in white light and exposed or not for 24h to supplemental narrowband UV-B followed by 15 min broadband UV-B.

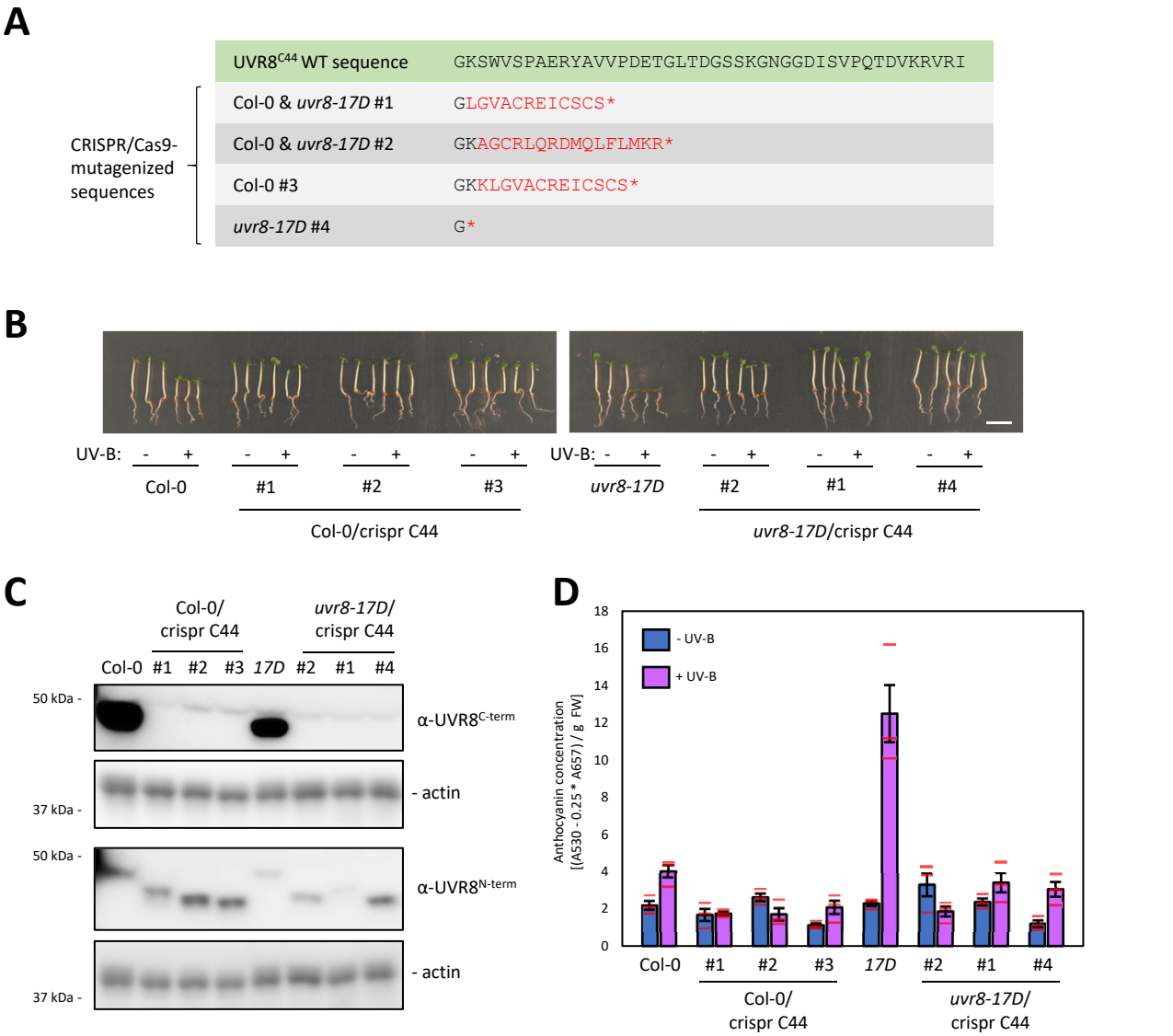

Fig. S7. Deletion of the VP motif–containing C-terminus of UVR8 abolishes the UV-B response in *uvr8-17D*. **(A)** Mutations induced by CRISPR/Cas9 directed against the *UVR8* sequence encoding the UVR8 C-terminus. The UVR8^{C44} wild-type sequence is shown, as well as the mutated sequences documented in Col-0 and/or *uvr8-17D* backgrounds. Residues generated as a consequence of frameshift are indicated in red, * indicates a newly formed translation stop codon. **(B)** Representative images of wild-type (Col-0) and *uvr8-17D* seedlings alongside three respective independent mutant lines containing CRISPR/Cas9-generated C-terminal C44 truncations (Col-0/crispr C44 #1–3, and *uvr8-17D*/crispr C44 #2, #1, and #4) grown in white light or white light supplemented with UV-B. Bar = 5 mm. **(C)** Immunoblot analysis of UVR8 and actin (loading control) protein levels in the lines described in (B) (*uvr8-17D* = *17D*). For analysis of UVR8 levels, antibodies specifically recognizing the N-terminus (α-UVR8$^{N\text{-term}}$ = α-UVR8$^{1\text{-}15}$) or the C-terminus (α-UVR8$^{C\text{-term}}$ = α-UVR8$^{426\text{-}440}$) of UVR8 were used. **(D)** Anthocyanin concentration in the lines described in (B); values of independent measurements (red bars), means, and SEM are shown (*N* = 3).

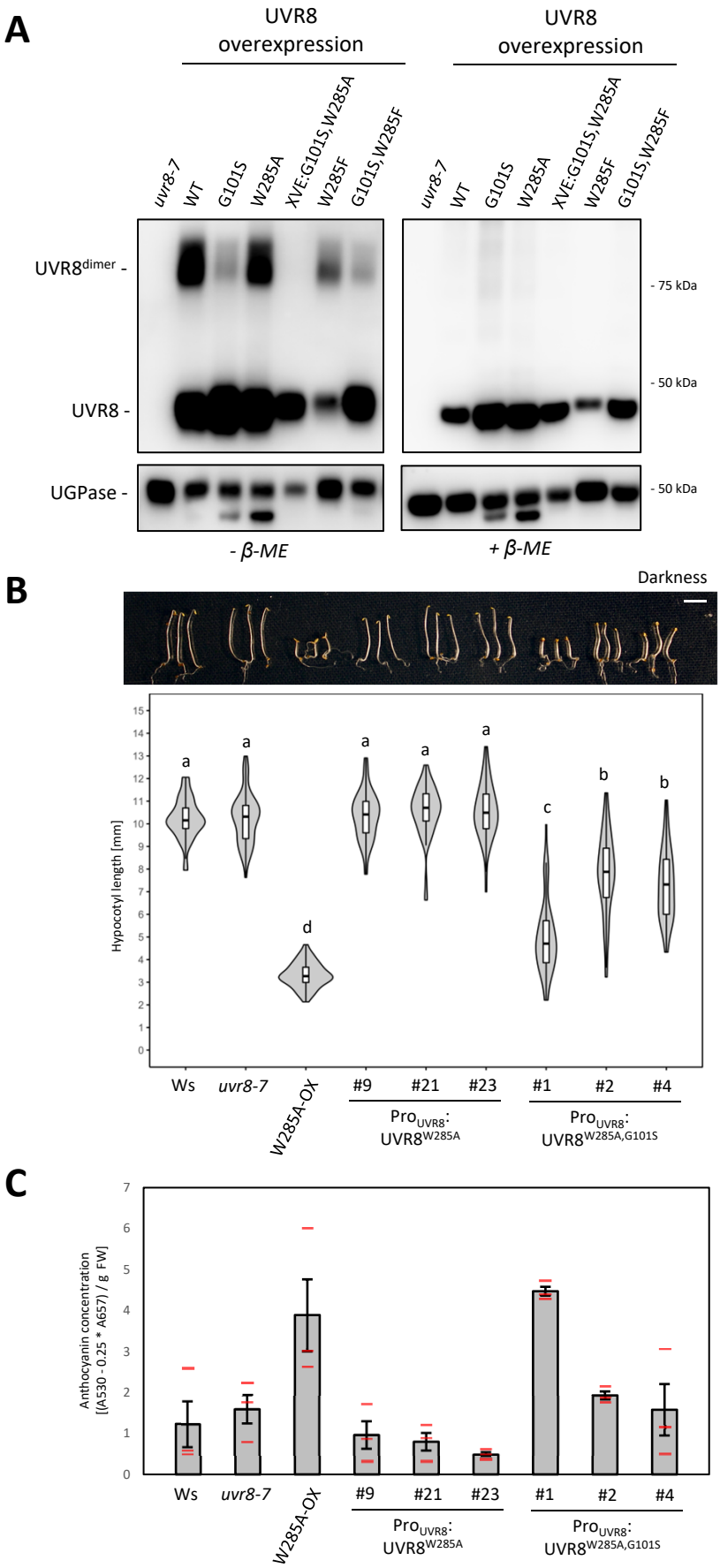

Fig. S8. Characterization of UVR8^{G101S,W285A} lines. **(A)** Dimer/monomer status of UVR8 from DSP-crosslinked extracts of various UVR8-overexpressing lines under a 35S or XVE-responsive promoter. UVR8^{W285A}- and XVE:UVR8^{G101S,W285A}-expressing lines were grown on 5 µM estradiol. Crosslinking was reversed by addition of 5% β-mercaptoethanol. UGPase is shown as loading control. **(B)** Representative images and quantification of hypocotyl length of seedlings of wild type (Ws), *uvr8-7*, *uvr8-7*/Pro$_{35S}$:UVR8^{W285A} (W285A-OX), and three independent lines each of *uvr8-7*/Pro$_{UVR8}$:UVR8^{W285A} (#9, #21, and #23) and *uvr8-7*/Pro$_{UVR8}$:UVR8^{G101S,W285A} (#1, #2, and #4) grown in darkness (N > 60). Shared letters indicate no statistically significant difference in the means (P > 0.05). Bar = 5 mm. **(C)** Anthocyanin concentration in the lines described in (B). Values of independent measurements (red bars), means, and SEM are shown (N = 3).

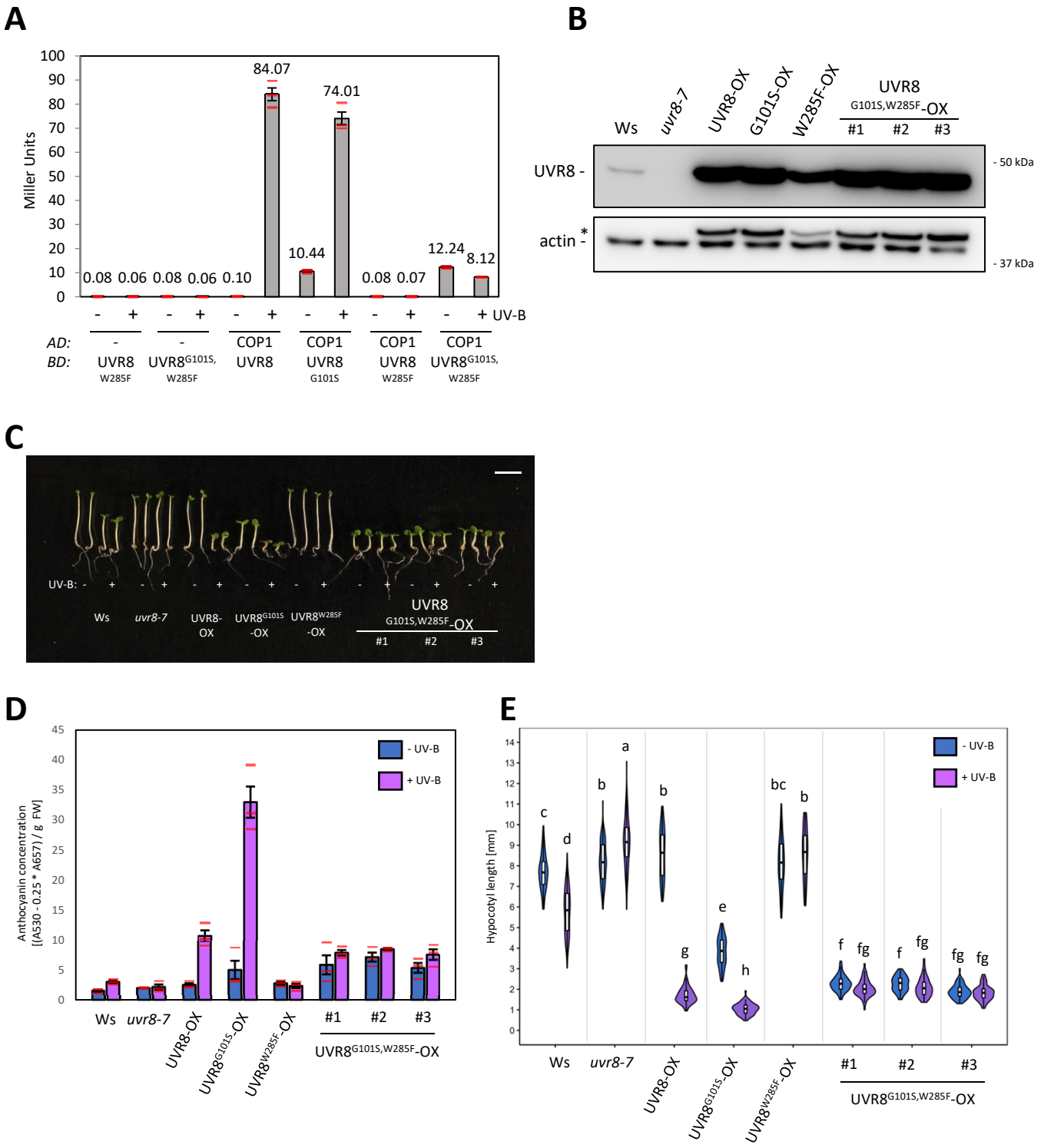

Fig. S9. Overexpression of UVR8^{G101S,W285F} results in weak constitutive photomorphogenesis similar to non-UV-B exposed UVR8^{G101S}. **(A)** Quantitative Y2H analysis of the interaction between COP1 and UVR8, UVR8^{G101S}, UVR8^{W285F}, and UVR8^{G101S,W285F} in the absence of UV-B. AD, activation domain; BD, DNA binding domain. **(B)** Immunoblot analysis of UVR8 and actin (loading control) protein levels in wild type (Ws), *uvr8-7*, *uvr8-7*/Pro$_{35S}$:UVR8 (UVR8-OX), *uvr8-7*/Pro$_{35S}$:UVR8^{G101S} #2 (G101S-OX), *uvr8-7*/Pro$_{35S}$:UVR8^{W285F} (W285F-OX), and three independent lines of *uvr8-7*/Pro$_{35S}$:UVR8^{G101S,W285F} (#1–3). Asterisk indicates residual UVR8 signal after stripping of the PVDF membrane. **(C)** Representative images of seedlings described in (B) grown for 4 d in white light or white light supplemented with UV-B. Bar = 5 mm. **(D)** Anthocyanin concentration in seedlings described in (C). Values of independent measurements (red bars), means, and SEM are shown (N = 3). **(E)** Quantification of hypocotyl length in seedlings described in (C) (N > 60). Shared letters indicate no statistically significant difference in the means (P > 0.05).

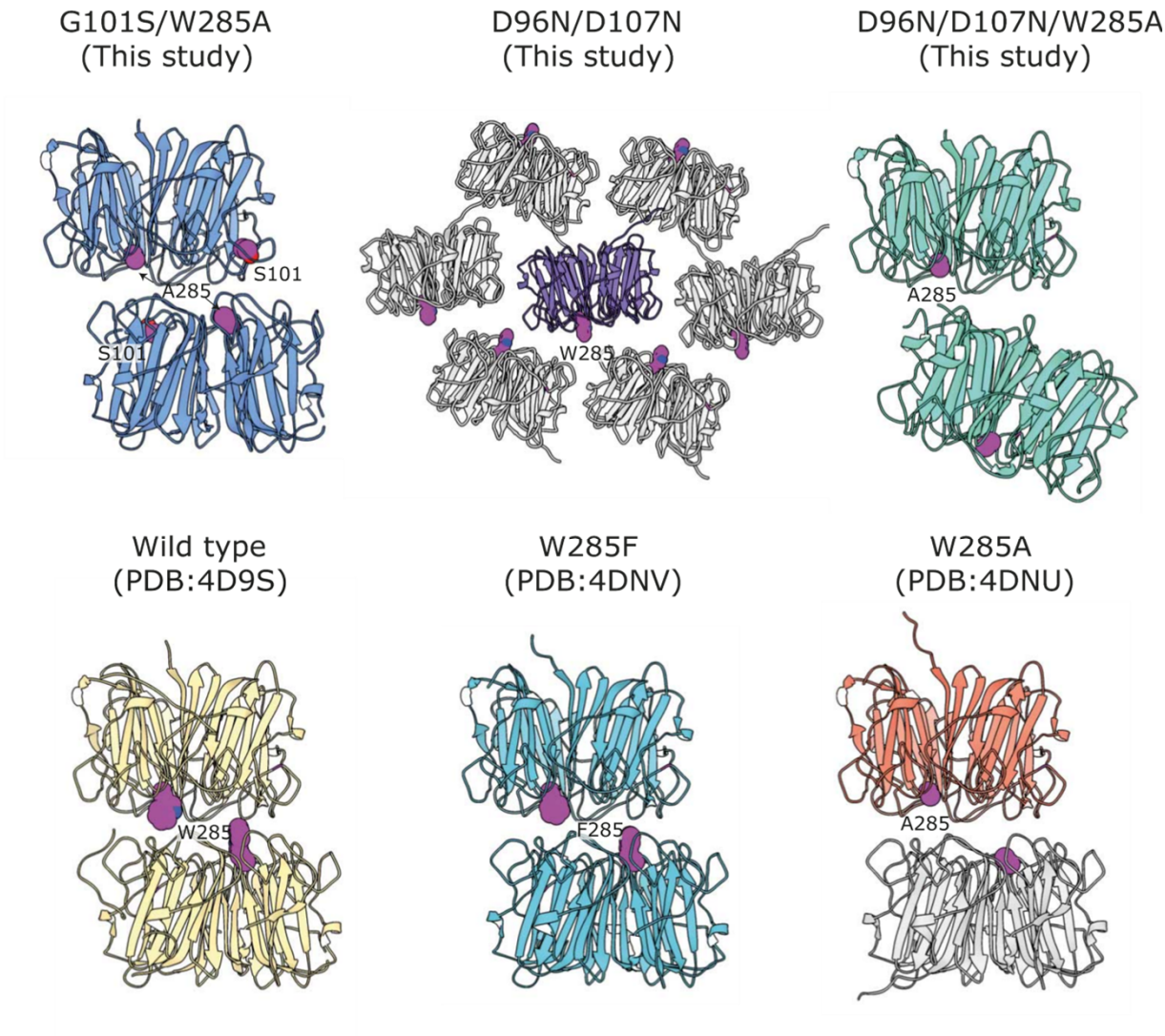

Fig. S10. Lattice interactions in different UVR8 variant crystal forms. UVR8 variants are depicted with colors and each represents the UVR8 present in one unit cell. Crystallographic symmetry partners are generated and depicted in gray to show higher-order assemblies when necessary. The residues at position 285 or 101 are highlighted in magenta spheres for orientation. $UVR8^{G101S,W285A}$ (G101S/W285A), UVR8 (wild type), and $UVR8^{W285F}$ (W285F) crystallize as conventional 'wild-type' (top-to-top) symmetric dimers. $UVR8^{W285A}$ (W285A) crystallizes with one molecule in the asymmetric unit, but form a canonical UVR8 dimer by symmetry within the crystal lattice. $UVR8^{D96N,D107N}$ (D96N/D107N) crystallizes also as a monomer and its symmetry mates show various conformations that do not correspond to a dimer. $UVR8^{D96N,D107N,W285A}$ (D96N/D107N/W285A) crystallizes as an unconventional top-to-bottom dimer.

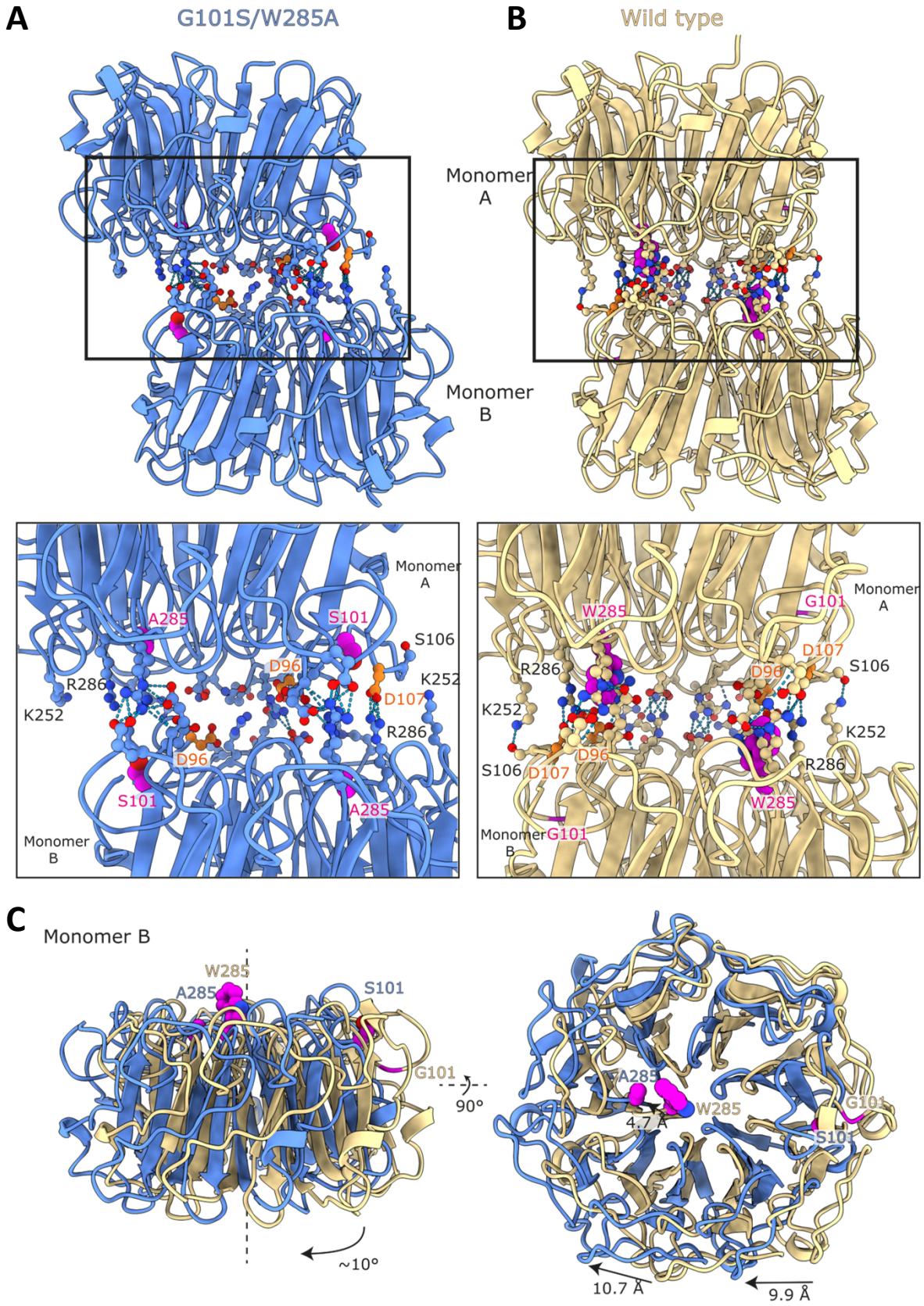

Fig. S11. UVR8^{G101S,W285A} is an asymmetric dimer with an altered dimeric interface compared to wild-type UVR8. **(A,B)** A comparison of the UVR8^{G101S,W285A} (G101S/W285A) and UVR8 (wild type) homodimer orientation based upon the superposition of monomer A. Monomer B of UVR8^{G101S,W285A} is rotated relative to the wild type (see (C)). Both structures are depicted as ribbons (UVR8^{G101S,W285A}, blue; wild-type UVR8, yellow). All side chains are depicted as ball-and-stick models. The sites of mutation residues 101 and 285 are colored in magenta. D96 and D107 are highlighted in orange. Hydrogen bonds or salt-bridges are colored in teal. The salt-bridges found in the symmetrical UVR8 dimer are no longer present in UVR8^{G101S,W285A}. A list of interaction residues is shown in Table S2. **(C)** Comparison of monomer B of UVR8^{G101S,W285A} and UVR8 homodimers based on the superposition of monomer A (as in (A)). Monomer B of UVR8^{G101S,W285A} is rotated ~10° and shows shifts of up to 10.7 Å relative to monomer B of a UVR8 dimer.

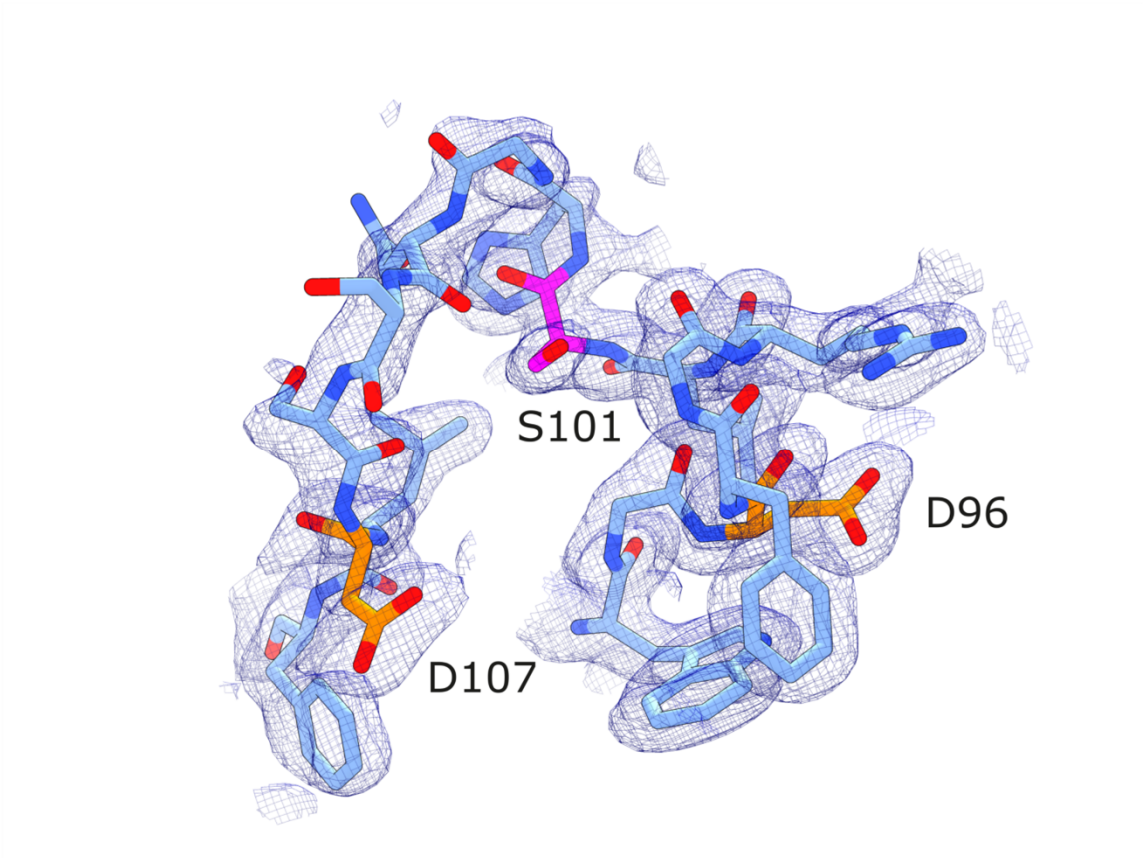

Fig. S12. Details of the G101S-containing loop region in UVR8. Shown is the loop containing the G101S mutation from chain A of the UVR8^{G101S,W285A} structure (in bonds representation, in blue). A 2mFo-DFc electron density map contoured around all atoms depicted at a level of 1 σ is shown alongside (blue mesh). The site of mutation, G101S, is highlighted in magenta. Important residues D96 and D107 are highlighted in orange.

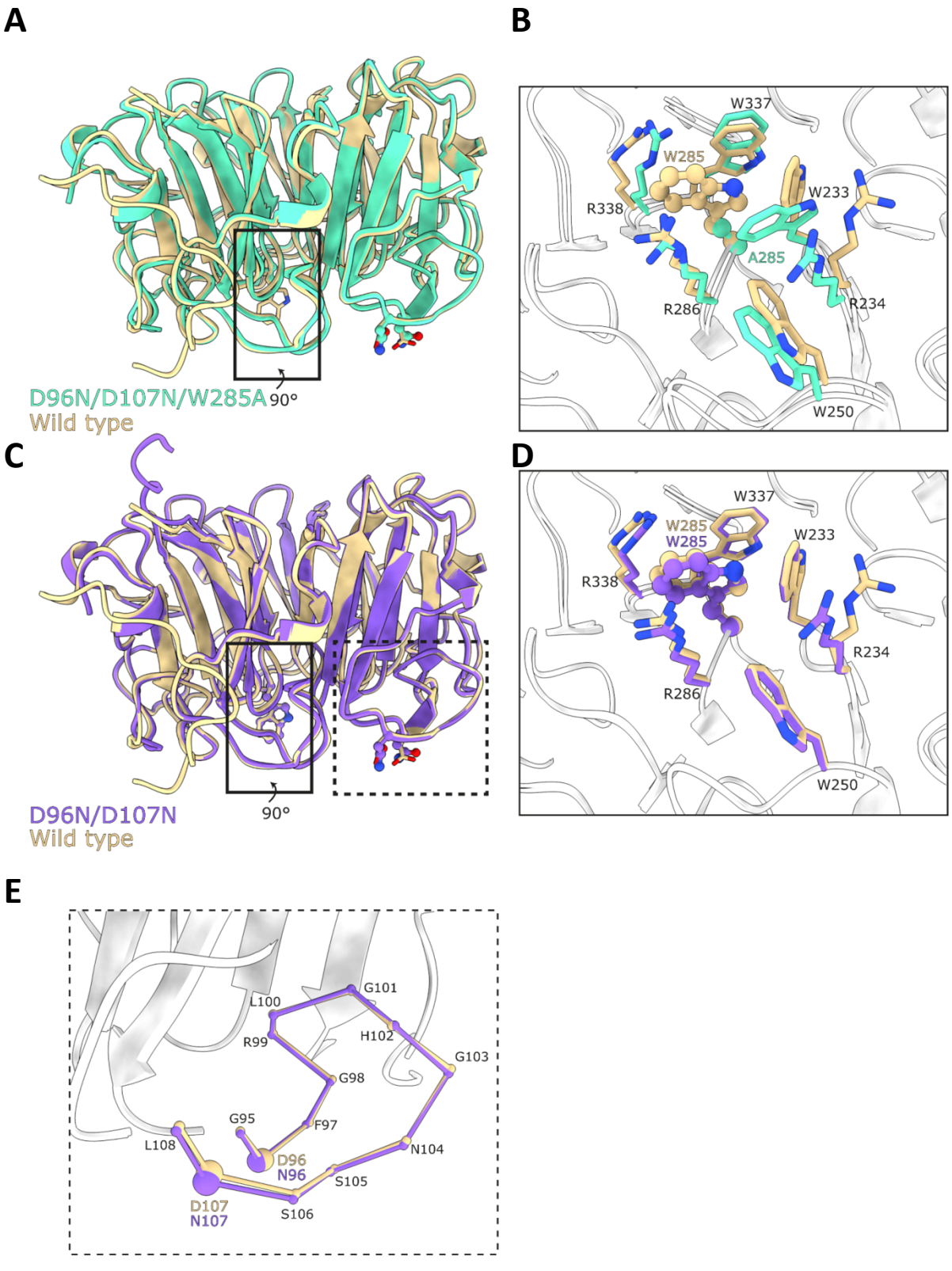

Fig. S13. UVR8^{D96N,D107N} shows no major structural changes. **(A,C)** Superposition of UVR8^{D96N,D107N,W285A} (D96N/D107N/W285A; green) or UVR8^{D96N,D107N} (D96N/D107N; purple) with a wild-type UVR8 (wild type; yellow) in ribbon representation. The sites of mutation, residues 96, 107 and 285, are represented by a ball-and-stick model. **(B,D)** A zoomed in view of the site containing the W285A mutation. The site of mutation is represented as a ball-and-stick model and the surrounding residues are shown as sticks. **(E)** Zoomed-in view of the loop containing the D96N,D107N mutations. The loop is represented as a ball-and-stick model to highlight the loop with each ball corresponding to a Cα carbon.

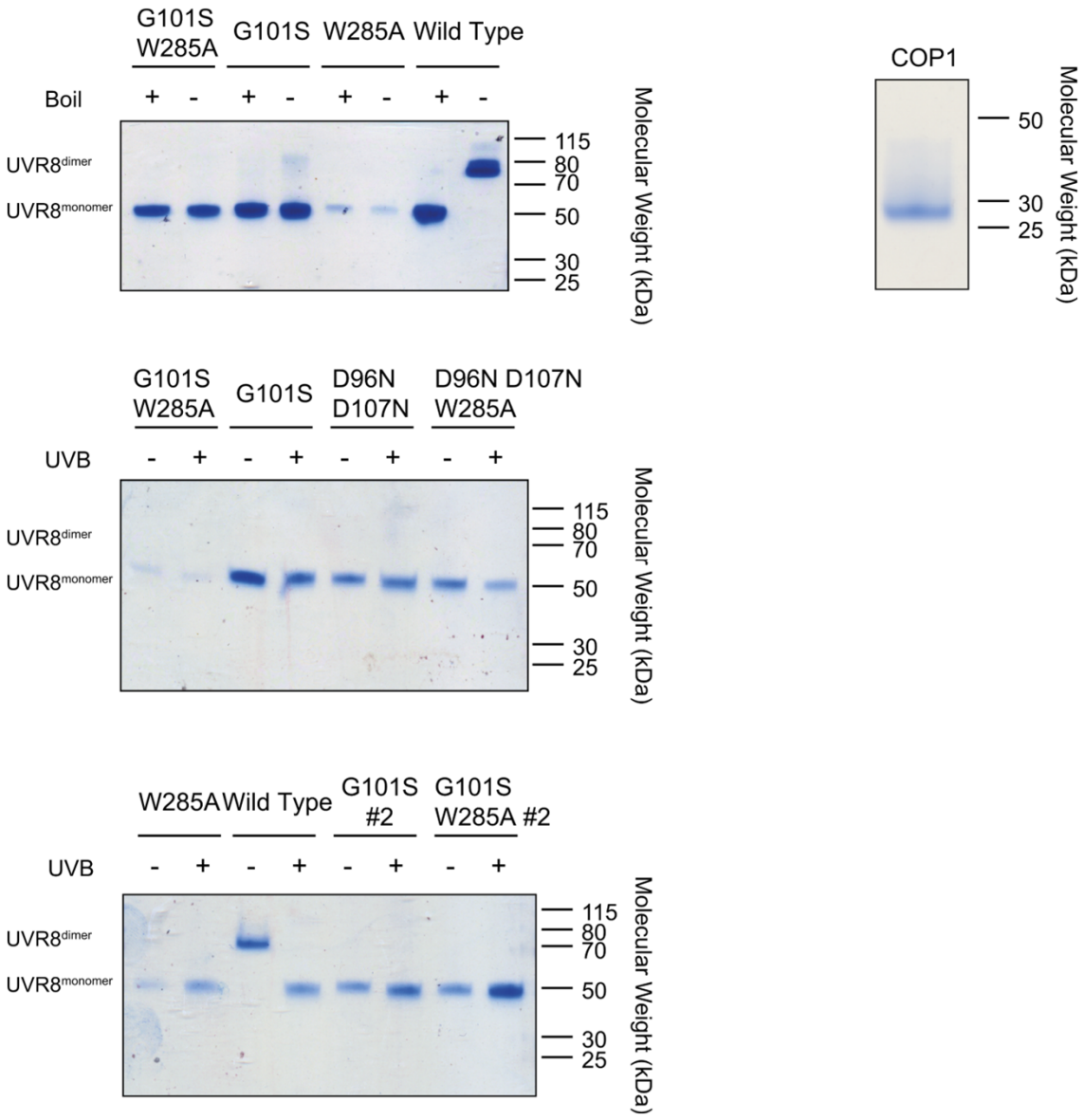

Fig. S14. Coomassie-stained 10% SDS-PAGE gels of purified proteins show high purity. Representative SDS-PAGE gels of proteins used in this study. "#2" in the bottom panel indicates proteins from a second batch of purification.

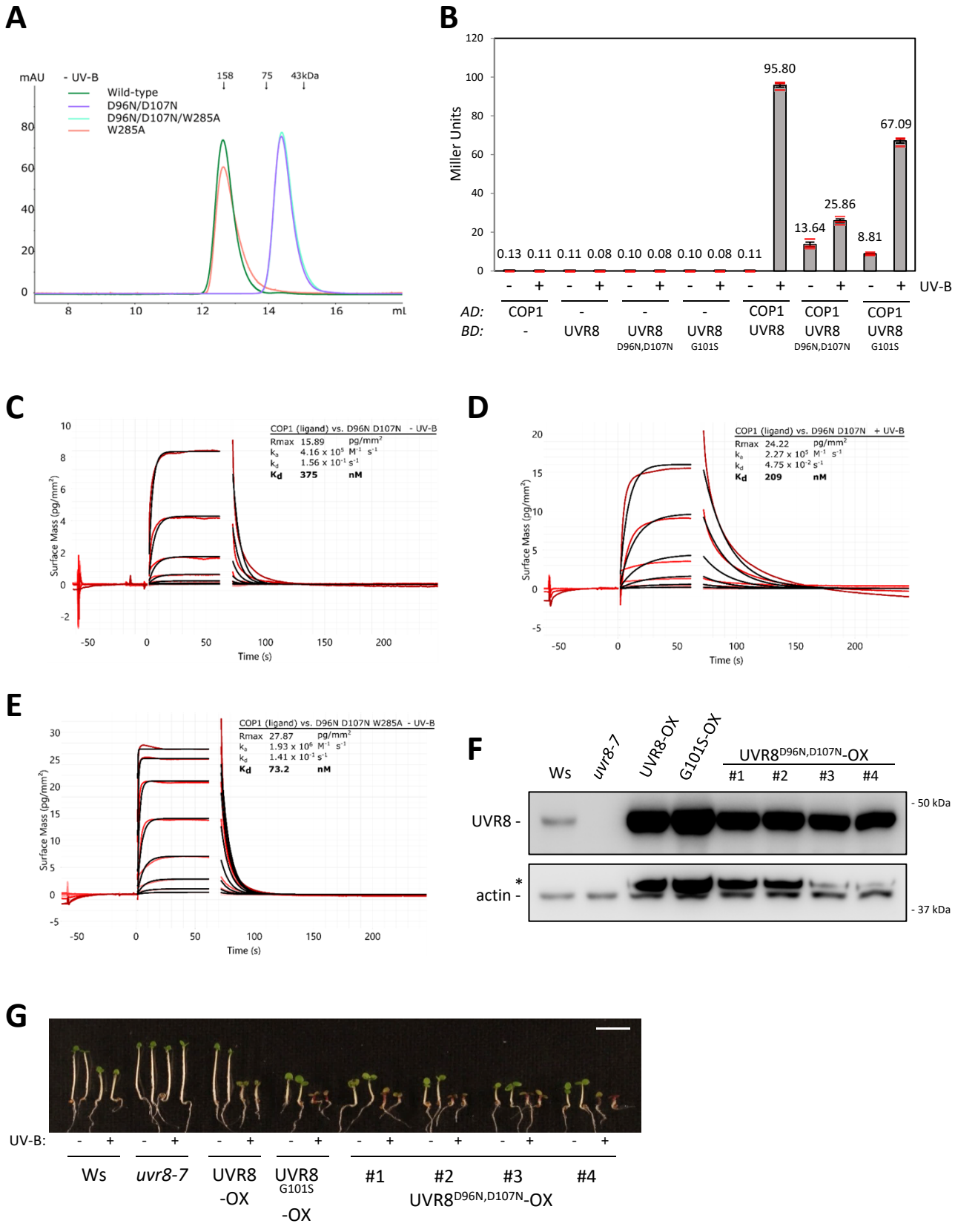

Fig. S15. Lines overexpressing UVR8^{D96N,D107N} phenocopy UVR8^{G101S}-overexpression lines. **(A)** Size-exclusion chromatography assay of recombinant UVR8 (wild-type), UVR8^{D96N,D107N}, UVR8^{W285A}, and UVR8^{D96N,D107N,W285A} proteins expressed in Sf9 insect cells. **(B)** Quantitative Y2H analysis of the interaction of COP1 with UVR8, UVR8^{D96N,D107N}, and UVR8^{G101S} in the absence or presence of UV-B. AD, activation domain; BD, DNA binding domain. **(C-E)** Binding kinetics of the full-length UVR8^{D96N,D107N} and UVR8^{D96N,D107N,W285A} versus the COP1 WD40 domain obtained by GCI experiments. Sensorgrams of protein injected are shown in red, with their respective heterogenous ligand binding model fits in black. The following amounts were typically used: ligand, COP1 (2000 pg/mm^2); analyte, UVR8 (2 µM highest concentration). ka = association rate constant, kd = dissociation rate constant, Kd = dissociation constant. **(F)** Immunoblot analysis of UVR8 and actin (loading control) protein levels in wild type (Ws), *uvr8-7*, *uvr8-7*/Pro$_{35S}$:UVR8 (UVR8-OX), *uvr8-7*/Pro$_{35S}$:UVR8^{G101S} #2 (G101S-OX), and four independent lines of *uvr8-7*/Pro$_{35S}$:UVR8^{D96N,D107N} (UVR8^{D96N,D107N}-OX #1–4). **(G)** Representative images of seedlings described in **f** grown for 4 d in white light or white light supplemented with UV-B. Bar = 5 mm.

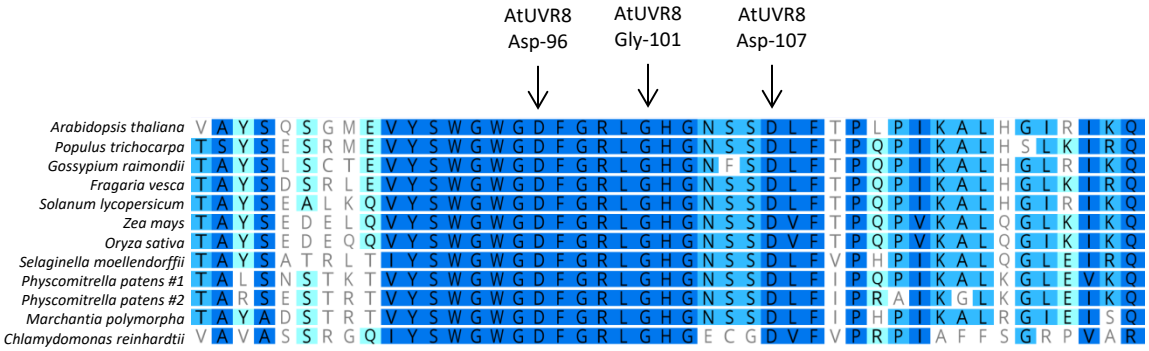

Fig. S16. Alignment of amino acid sequences from various UVR8 orthologs. Sequences were retrieved using protein BLAST from the Phytozome resource (phytozome.jgi.doe.gov). Sequences were aligned using the Geneious software. Conservation of residues is indicated by blue coloration. Residues corresponding to Arabidopsis Asp-96, Gly-101 and Asp-107 residues are highlighted.

Table S1. Data collection and refinement statistics.

UVR8 Variant	D96N D107N	D96N D107N W285A	G101S W285A
	native	*native*	*native*
Data collection			
Space group	*C* 1 2 1	*P* 3_2 2 1	*P* 2 2_1 2_1
a, b, c (Å)	97.61, 50.98, 70.49	98.27, 98.27, 138.84	50.54, 99.12, 132.73
α, β, γ (°)	90, 104.95, 90	90, 90, 120	90, 90, 90
Resolution (Å)	44.85 - 1.39 (1.44 - 1.39)	49.13 - 2.1 (2.18 - 2.1)	40.21 - 1.75 (1.81 - 1.75)
R_{meas} [#]	0.1091 (1.35)	0.1875 (3.137)	0.07952 (2.09)
Mean I/σI[#]	8.97 (1.37)	13.81 (1.04)	21.71 (1.37)
Completeness (%)[#]	99.96 (99.93)	99.95 (99.96)	98.68 (97.23)
Multiplicity[#]	6.6 (6.1)	20.1 (18.9)	13.4 (12.8)
CC1/2[#]	0.996 (0.599)	0.999 (0.483)	1 (0.659)
Refinement			
Resolution (Å)	44.85 - 1.39	49.13 - 2.1	40.21 - 1.75
Total reflections	443834	920407	897941
R_{work} [#]	0.1439 (0.2697)	0.1970 (0.3365)	0.1553 (0.2818)
R_{free} [#]	0.1793 (0.3124)	0.2481 (0.3504)	0.2197 (0.3574)
Number of non-hydrogen atoms	3095	5621	5888
macromolecules	2858	5498	5613
ligands	6	47	39
solvent	231	76	236
Protein residues	373	734	728
RMS deviations (bonds)[#]	0.01	0.011	0.01
RMS deviations (angles)[#]	1.03	1.14	1.06
Average B-factor[#]	23.40	48.52	40.99
macromolecules	22.74	48.54	40.80
ligands	37.07	55.22	69.33
solvent	31.16	43.21	40.85
PDB	**6XZL**	**6XZM**	**6XZN**

Statistics for the highest-resolution shell are shown in parentheses.
[#]as defined by phenix.table_one and phenix.model_vs_data

Table S2: List of residues forming hydrogen bonds and salt-bridges at the UVR8^{G101S,W285A} and UVR8 dimer interface. Pairs colored black represent reciprocal interactions found between monomers of either UVR8^{G101S,W285A} or UVR8. Red pairs are non-reciprocal pairs between monomers. The wild-type UVR8 forms a symmetric dimer. Interaction pairs noted with an asterisk (*) denote interactions that are unique to the UVR8^{G101S,W285A} dimer or to the wild-type dimer.

G101S W285A			**Wild type**		
Hydrogen Bonds and Salt Bridges			Hydrogen Bonds and Salt Bridges		
Chain A	**Chain B**		**Chain A**	**Chain B**	
Glu43	Arg338		Glu43	Arg338	
Glu43	Arg354		Glu43	Arg354	
Glu43	Thr356	*			
Asp44	Arg338		Asp44	Arg338	
			Ala52	Arg354	*
Glu53	Arg354		Glu53	Arg354	
			Asp96	Arg286	*
Arg99	Asn149	*			
Arg99	Glu182	*			
			Ser106	Lys252	*
Asp107	Arg286		Asp107	Arg286	
Arg146	Gln148	*	Arg146	Glu182	
Arg146	Glu182				
			Gln148	Asn149	*
			Asn149	Gln148	*
			Thr157	Arg200	*
			Glu158	Arg200	*
Asp159	Gln148	*			
Glu182	Arg99	*			
			Glu182	Arg146	
			Arg200	Thr157	*
			Arg200	Glu158	*
			Lys252	Ser106	*
			Arg286	Asp96	*
			Arg286	Asp107	
Arg338	Glu43		Arg338	Glu43	
Arg338	Asp44		Arg338	Asp44	
Arg354	Glu43		Arg354	Glu43	
			Arg354	Ala52	*
Arg338	Glu53		Arg354	Glu53	